Available online at www.sciencedirect.com
ScienceDirect
Journal of Nuclear Materials 374 (2008) 293–297
journal of nuclear materials
www.elsevier.com/locate/jnucmat

# Electron spin resonance measurement of radiation-induced defects and reactions in vitreous silica irradiated with ion beams

Jun Takemoto, Kimikazu Moritani, Ikuji Takagi, M. Akiyoshi, Hirotake Moriyama *

*Department of Nuclear Engineering, Graduate School of Engineering, Kyoto University, Yoshida, Sakyo-ku, Kyoto 606-8501, Japan*

Received 1 June 2007; accepted 27 August 2007

**Abstract**

The electron spin resonance (ESR) measurement of irradiation defects and reactions in ion beam irradiated vitreous silica was performed. The spin densities of E′ centers, non-bridging oxygen hole centers (NBOHCs), and peroxy radicals (PORs) were measured as a function of the ion beam fluence and postirradiation isothermal annealing temperature. The spin densities of these centers were observed to saturate above the dpa value of $10^{-2}$. In isothermal annealing experiments, sequential reactions of the E′ centers with oxygen atoms to form the NBOHCs and PORs were observed to occur, and the rate constants of those reactions were determined. The activation energies were obtained to be about 0.4 eV for those reactions.


*PACS:* 61.80.Jh; 61.72.Cc

## 1. Introduction

In the case of vitreous silica, three fundamental centers of E′ center (≡Si•), peroxy radical (POR: ≡Si—O—O•) and non-bridging oxygen hole center (NBOHC: ≡Si—O•) are known to form the basis of the present understanding of defects in this material [1]. Those are all paramagnetic and have been well characterized by electron spin resonance (ESR) techniques, compared with the diamagnetic oxygen-deficiency centers (ODCs: ≡Si:Si≡). However, the reaction kinetics of those centers is considered to be one of the remaining problems, and the quantitative database is needed for the performance assessment of this material in the strong radiation field in such proposed fusion reactors.

In our previous study [2], the ESR measurement of radiation-induced defects in ion beam irradiated vitreous silica was performed to study the effects of the ion beam fluence. The results of the ion beam irradiation were compared with those of neutron irradiation [3] in order to discuss the reaction mechanism of the radiation-induced defects. It was observed that the spin densities of the E′s, NBOHCs, and PORs increase with increasing dpa value and that, above the dpa value of $10^{-2}$, all the spin densities become saturated. Cascade overlaps by ion beam irradiation were thus considered to be responsible for this saturation behavior. For the reaction kinetics of those centers, an isochronal annealing experiment was also performed, and the sequential reactions of the E′ centers with oxygen atoms to form the NBOHCs and PORs were observed to occur, as suggested in the literature [4]. Unfortunately, however, the rate constants of these reactions were not determined yet.

In order to obtain the reaction rate constants of radiation-induced defects, the ESR measurement of radiation-induced defects in ion beam irradiated vitreous silica was performed in the present study. The spin densities of the E′s, NBOHCs and PORs were measured as a function of the postirradiation isothermal annealing temperature, and the reaction rate constants of those centers were determined. The saturation behavior of radiation-induced defects was also discussed by using the determined rate constants.

* Corresponding author. Tel./fax: +81 75 753 5824.
*E-mail address:* moriyama@nucleng.kyoto-u.ac.jp (H. Moriyama).

0022-3115/$ - see front matter © 2007 Elsevier B.V. All rights reserved.
doi:10.1016/j.jnucmat.2007.08.011

## 2. Experimental

Specimens of vitreous silica, T-2030 (1 ppm OH) and T-4040 (800 ppm OH), were obtained from Toshiba Ceramics Co., which were of 10 mm in diameter and about 0.5 mm in thickness. Specimens were irradiated at room temperature with a $He^+$ ion beam, accelerated to 2 MeV with a Van de Graaff accelerator. The range and total number of displacements were estimated to be about 8 μm and 160 displacements/ion, respectively, by using the TRIM code (SRIM-98) with the displacement energies of 20 eV for Si and O. Also, by considering inhomogeneous defect production and by taking a weighted average value for dpa, a conversion factor of $4.1 \times 10^{20}$ ions $m^{-2}$ $dpa^{-1}$ for oxygen was obtained for 2 MeV $He^+$ ions. The size of the ion beam was about 3 mm in diameter and its intensity was monitored. The ion beam intensity ranged from $6.0 \times 10^{-4}$ to $1.3 \times 10^{-3}$ A $m^{-2}$, and the dose ranged from $5.0 \times 10^{18}$ to $2.2 \times 10^{20}$ ions $m^{-2}$ (0.012–0.54 dpa). As reported previously [2], no apparent effect of the ion beam intensity was observed on each spin density. A thermocouple was attached to the sample surface to monitor its temperature at a distance close to beam area. In the irradiation at room temperature, the temperature rise by beam heating was observed to be within a few degrees as estimated by taking the values of thermal diffusion coefficient, density and heat capacity of silica.

After the irradiation, first-derivative ESR spectra were recorded either at room temperature (for the E′s) or at 77 K (for others) on a JEOL JES-TE200 instrument operating at X-band frequencies ($\nu \sim 9.26$ GHz) with 100-kHz magnetic field modulation. Measurements of the *g*-values were accomplished by using conventional standard samples of DPPH (diphenylpicrylhyrazyl) and MgO. Isothermal annealing experiments at 373 K, 423 K, 473 K and 523 K were carried out by moving the samples contained in fused quartz sample tubes to an external furnace. Spin concentrations were determined by resolution of derivative spectra into a number of components, double numerical integration of every component spectra and comparison of the obtained areas with that of a DPPH sample of $1.53 \times 10^{21}$ spins $g^{-1}$. The accuracy of the numerical integrations was typically of the order of ±5% for the stronger signals in the irradiated samples. In the case of the weaker signals, these errors were over ±10% due to low signal-to-noise ratios.

## 3. Results and discussion

### 3.1. Resolution of ESR spectra

Fig. 1 shows a typical ESR spectrum of ion beam irradiated vitreous silica of T-2030. As shown in this figure, the resolution of the observed spectra was well completed by only considering the participation of the well-known paramagnetic defect centers of the E′, NBOHC and POR. In the resolution of each spectrum, the initial g-values and

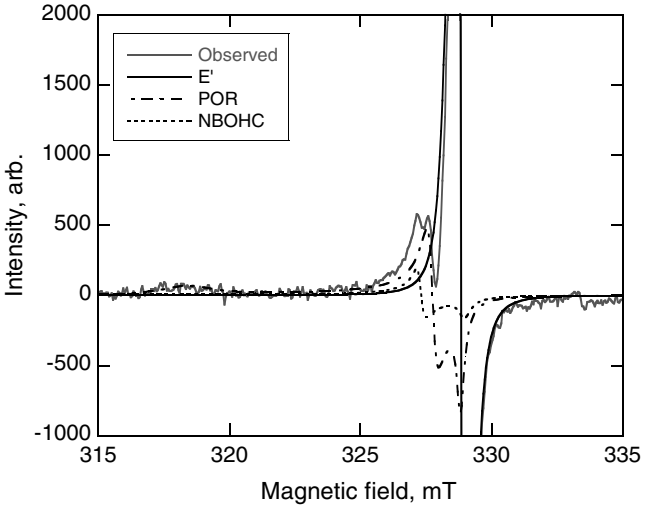


Fig. 1. Typical X-band ESR spectrum of the 2 MeV $He^+$ irradiated vitreous silica (T-2030) and its components.

Table 1
*g*-values and peak-to-peak derivative widths determined in the present analysis

| Defects | *g*-value | | | Peak-to-peak derivative width | | |
|---|---|---|---|---|---|---|
| | $g_1$ | $g_2$ | $g_3$ | $\sigma_1$ | $\sigma_2$ | $\sigma_3$ |
| E′ | 2.0003 | 2.0005 | 2.0017 | 0.05 | 0.05 | 0.05 |
| POR | 2.002 | 2.007 | 2.067 | 0.1 | 0.2 | 1 |
| NBOHC | 2.001 | 2.010 | 2.08 | 0.1 | 0.3 | 3 |

peak-to-peak derivative widths of Lorentzian line shapes for the E′, NBOHC and POR were taken from our previous study [2,3]. A line shape simulation was performed similar to the case in the literatures [5–7], and a least squares fitting method was applied to the simulation in order to determine the *g*-values and peak-to-peak derivative widths of the component defects. The results are summarized in Table 1.

### 3.2. Effect of ion beam fluence

Fig. 2 shows the effects of ion beam fluence on the spin densities of the E′s, NBOHCs, and PORs. It is seen that the spin densities of the E′s, NBOHCs, and PORs increase with increasing dpa value. Above the dpa value of $10^{-2}$, however, all the spin densities become saturated. As already reported [2], cascade overlaps are considered to be responsible for this saturation behavior, and defect clusters may be produced in this region. The observed saturation behaviors of the E′s, NBOHCs, and PORs are discussed later by taking into account the reaction rate constants which are determined below.

### 3.3. Isothermal annealing behaviors

Fig. 3 shows the results obtained from the isothermal annealing experiments with T-2030 irradiated by 2 MeV

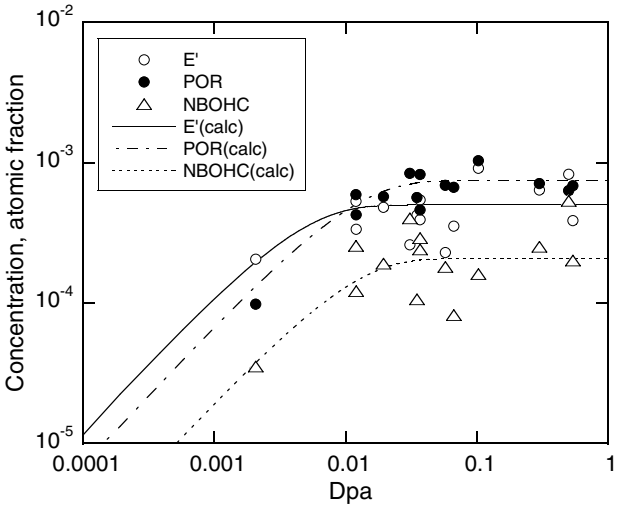


Fig. 2. Dpa dependence of spin densities in the 2 MeV $He^+$ irradiated vitreous silica (T-2030). Ion beam intensity: around $6.0\times10^{-4}$ to $1.3\times10^{-3}$ A $m^{-2}$. Open circles: E′, full circles: POR, squares: NBOHC, triangles. Curves represent the calculated results. See text for details.

$He^+$ ions. As seen in this figure, the spin densities of the E′s and NBOHCs decrease and those of the PORs increase with the annealing time. Similar results were also obtained for T-4040. It is important to note that the total spin densities of the E′s, NBOHCs and PORs are not changed but almost constant during each annealing experiment. This fact strongly suggests that the E′s and NBOHCs are converted to the PORs by annealing as [2–4]:

$$E' + O \rightarrow NBOHC \quad (1)$$

$$NBOHC + O \rightarrow POR \quad (2)$$

It is known that the PORs are also produced from the *E′*s and $O_2$ molecules [8]. Because of rather high activation energy (1.17 to 1.35 eV [9]) for the $O_2$ diffusion, however, Griscom and Mizuguchi [4] pointed out that the reaction of the E′s with the $O_2$ hardly occurs at lower temperatures but that reactions (1) and (2) occur. The present results are well consistent with their expectation.

Since the total spin densities are almost constant, reactions other than (1) and (2) are considered to be less

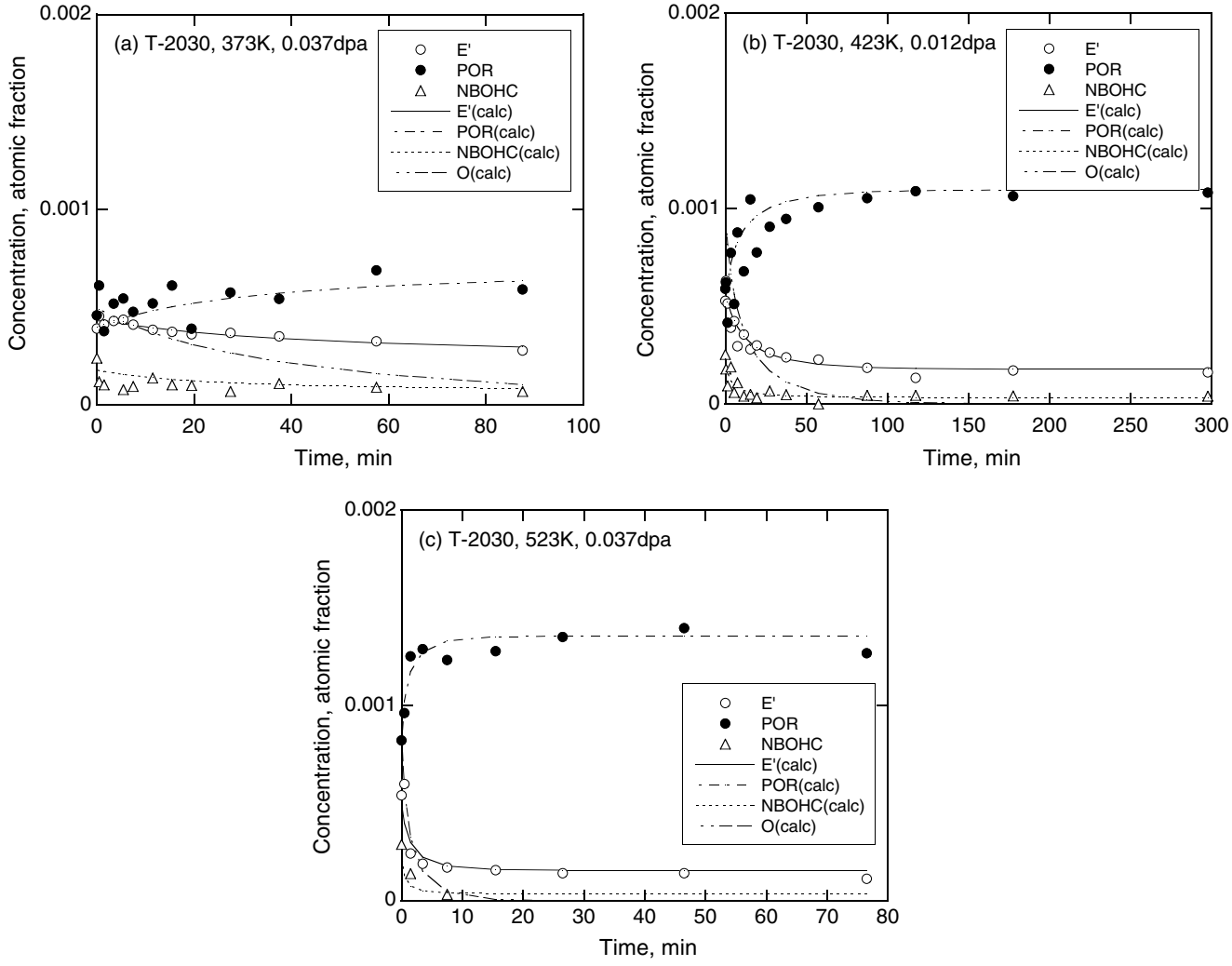


Fig. 3. Isothermal annealing behavior of radiation-induced defects in vitreous silica (T-2030) irradiated by 2 MeV $He^+$ ions at (a) 373 K, (b) 423 K, and (c) 523 K. Marks are experimental and curves represent the least-squares fits of the data to Eqs. (5).

important in the present experiments. The present observations are then analyzed by taking reactions (1) and (2). In this case, the variations of the spin densities of the E′s, NBOHCs and PORs with annealing time are calculated by solving the following equations:

$$d[E']/dt = -k_1[E'][O] \quad (3)$$

$$d[NBOHC]/dt = k_1[E'][O] - k_2[NBOHC][O] \quad (4)$$

$$d[POR]/dt = k_2[NBOHC][O] \quad (5)$$

where $k_1$ and $k_2$ are the rate constants of reactions (1) and (2), respectively. The values of the rate constants are given in atomic fraction in the present study. Eqs. (3)–(5) are solved by the Runge-Kutta method to obtain the densities of the E′s, NBOHCs and PORs, and the rate constants $k_1$ and $k_2$ are determined together with the initial density of the Os which is treated as another free parameter. In some trials in the present analysis, possible reactions of the Os such as $O + O \rightarrow O_2$ are taken into account together with reactions (1) and (2), but no improvement is obtained in the fitting results. It is confirmed that reactions (1) and (2) are enough to explain the observations.

As shown in Fig. 3, in which the calculated isothermal annealing behaviors are compared with the observations, good agreements are obtained in all the cases. The initial density of the Os is obtained to be $5 \times 10^{-4}$, $1 \times 10^{-3}$ and $9 \times 10^{-4}$ in atomic fraction in the specimens of Fig. 3 (a)–(c), respectively. The values are acceptable considering the possible scatters due to different specimens, similarly to the case of the E′s, PORs and NBOHCs in Fig. 2. For the formation of the Os, it may be remembered that the Os are likely formed with the ODCs by ion beam irradiation [9].

Fig. 4 (a) and (b) show the Arrhenius plots of the rate constants ($k_1$ and $k_2$) obtained for T-2030 and T-4040, respectively. As summarized in Table 2, the Arrhenius equations of the rate constants are obtained by the least-squares fitting, and the activation energies are obtained to be about 0.40 eV for every reaction of the Os in both specimen. Also, only slight differences are found for the pre-exponential term which is possibly due to different specimens. From the present results, it may be concluded that the activation energy for reactions of the Os in vitreous silica is about 0.40 eV and that no apparent difference is found due to the OH content in the specimen.

According to the literature [10], oxygen is generally considered to diffuse as the molecular $O_2$, and activation energies are given in the range of 1.17 to 1.35 eV by gas transport experiments, which are much higher than the present value for the O. In his calculation study [11], Hamann found the peroxy linkage as the lowest energy configuration of an atomic O in α-$SiO_2$, and proposed its diffusion with the peroxy exchange barrier of 1.3 eV. This value, which is not for vitreous $SiO_2$ but for crystalline $SiO_2$, is still high similarly to the $O_2$. For oxygen ions of $O^-$ and $O^{2-}$, on the other hand, Jin and Chang suggested that a double Si-O-Si bridge structure is the lowest energy configuration of those ions, and reported extremely low energy barriers of 0.11–0.27 eV in this case [12]. Also, Roma et al. considered such interactions as those of hydrogen impurities with the Os, although no conclusion was obtained for the consequences on oxygen diffusion [13]. In view of these various possibilities, further confirmation and consideration may be needed for details of the oxygen diffusion mechanism itself.

It is interesting and important to note that the present reaction scheme and obtained rate constants are consistent with the observed saturation behaviors of the E′s, NBOHCs and PORs, as shown in Fig. 2. In this case, the saturation behavior of the E′s, NBOHCs and PORs are calculated by taking the following equations:

$$d[E']/dt = g'_E(\phi/c) + k_1[E'][O] + k'_E(\phi/c)[E'] \quad (6)$$

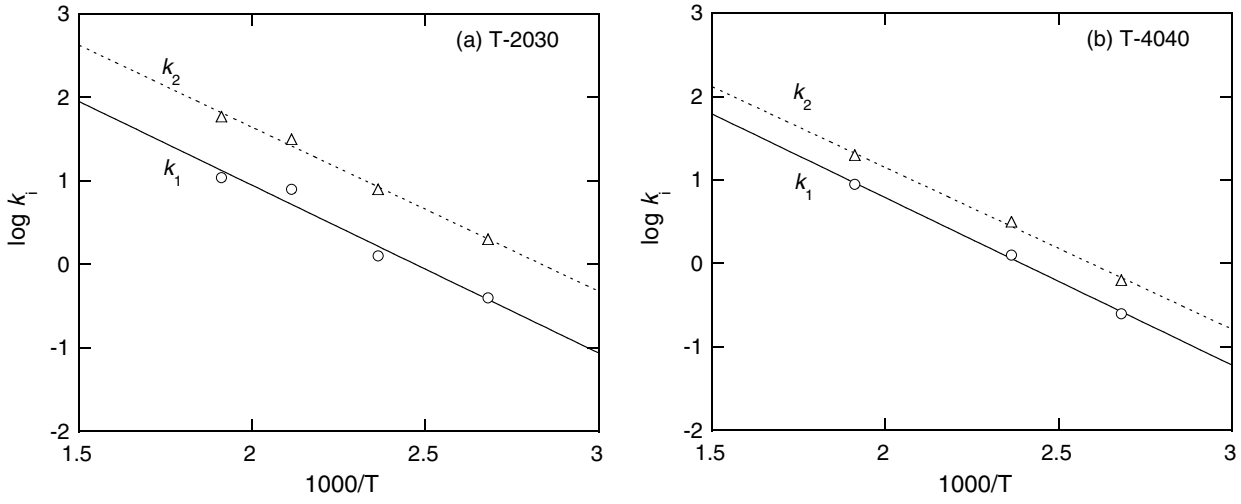


Fig. 4. Arrhenius plots of reaction rate constant $k_1$ and $k_2$ for (a) T-2030 and (b) T-4040. Marks are experimental and curves represent the least-squares fits of the data to the Arrhenius equations.

Table 2
Reaction rate constants obtained from the analysis of isothermal annealing data

| Specimen | Rate constants | $k_i = A_i \exp[-E_i/kT]$ | |
|---|---|---|---|
| | | $A_i$ (atomic fraction$^{-1}$ s$^{-1}$) | $E_i$ (eV) |
| T-2030 | $k_1$ | $10^{5.0\pm0.7}$ | $0.40 \pm 0.06$ |
| | $k_2$ | $10^{5.6\pm0.3}$ | $0.39 \pm 0.02$ |
| T-4040 | $k_1$ | $10^{4.8\pm0.2}$ | $0.40 \pm 0.02$ |
| | $k_2$ | $10^{5.0\pm0.3}$ | $0.38 \pm 0.02$ |

$$d[NBOHC]/dt = g_{NBOHC}(\phi/c) + k_1[E'] \times [O] - k_2[NBOHC][O] - k'_{NBOHC}(\phi/c) \times [NBOHC] \quad (7)$$

$$d[POR]/dt = g_{POR}(\phi/c) + k_2[NBOHC][O] - k'_{POR}(\phi/c)[POR] \quad (8)$$

$$d[O]/dt = g_O(\phi/c) - k_1[E'][O] - k_2[NBOHC] \times [O] - k'_O(\phi/c)[O] \quad (9)$$

where $g_{E'}$, $g_{NBOHC}$, $g_{POR}$ and $g_O$ represent the production rates (atomic fraction·dpa$^{-1}$) of the E′s, NBOHCs, PORs and Os by ion beam irradiation, respectively, $\varphi$ the ion beam intensity (ions m$^{-2}$ s$^{-1}$), $c$ the conversion factor ($4.1 \times 10^{20}$ ions m$^{-2}$ dpa$^{-1}$), and $k'$ the reaction rate constant (dpa$^{-1}$) of each defect by cascade overlaps. The $k_1$ and $k_2$ values are obtained from the present results in Fig. 3. For the fits of the data to Eqs. (9), the $g_{E'}$, $g_{NBOHC}$, $g_{POR}$ and $g_O$ values are obtained to be 0.12, 0.02, 0.05, and 0.12, respectively, and the $k'$ is obtained, as summarized in Table 3.

The calculated saturation behaviors agree well with the observed ones, as shown in Fig. 2. No apparent contribution of reactions (1) and (2) is found in the observed results because of the smaller $k_1$ and $k_2$ values at the irradiation temperature of 298 K. It is thus recognized that the saturation behaviors are mainly due to the reactions of each defect by cascade overlaps above the dpa value of $10^{-2}$. The reactions with the rate constant $k'$ may include not only the recombination of each defect with the newly formed ones but also the transformation to the higher order defects such as oxygen molecules and multivacancies, and there may be various types of defects in this dpa region. Considering that the contribution of reactions (1) and (2) will increase with increasing temperature, it is suggested to measure the saturation behaviors at the higher temperatures and the formation of the higher order defects in further studies.

Table 3
Parameter values for defect production and reactions by cascade overlaps

| Defect | $g$ (atomic fraction dpa$^{-1}$) | $k'$ (dpa$^{-1}$) |
|---|---|---|
| E′ | 0.12 | $10^{2.4}$ |
| POR | 0.05 | $10^{1.9}$ |
| NBOHC | 0.02 | $10^{1.8}$ |

## 4. Conclusions

In order to know the production and saturation behaviors of radiation-induced defects in vitreous silica, ESR measurements were performed in the present study. The spin densities of the E′s, NBOHCs, and PORs were observed to saturate above the dpa value of $10^{-2}$. In isothermal annealing experiments, the sequential reactions of the E′ centers with oxygen atoms to form the NBOHCs and PORs were observed to occur, and the rate constants of those reactions were determined. The activation energies were obtained to be about 0.4 eV for those reactions. The proposed reaction scheme and obtained rate constants were shown to be consistent with the observed saturation behaviors of radiation-induced defects in vitreous silica.

## References

[1] L. Skuja, J. Non-Cryst. Solids 239 (1998) 16.
[2] K. Moritani, Y. Teraoka, I. Takagi, H. Moriyama, J. Nucl. Mater. 329–333 (2004) 988.
[3] K. Moritani, I. Takagi, H. Moriyama, J. Nucl. Mater. 325 (2004) 169.
[4] D.L. Griscom, M. Mizuguchi, J. Non-Cryst. Solids. 239 (1998) 66.
[5] R.A.B. Devine, Phys. Rev. 35 (1987) 9783.
[6] D.L. Griscom, J. Non-Cryst. Solids 149 (1992) 137.
[7] T. Tabata, M. Hasegawa, M. Fujinami, Y. Ito, H. Sunaga, S. Okada, S. Yamaguchi, J. Nucl. Mater. 239 (1996) 228.
[8] A.H. Edwards, W.B. Fowler, Phys. Rev. B26 (1982) 6649.
[9] K. Moritani, I. Takagi, H. Moriyama, J. Nucl. Mater. 312 (2003) 97.
[10] M.A. Lamkin, F.L. Riley, R.J. Fordham, J. Eur. Ceram. Soc. 10 (1992) 347.
[11] D.R. Hamann, Phys. Rev. Lett. 81 (1998) 3447.
[12] Y.-G. Jin, K.J. Chang, Phys. Rev. Lett. 86 (2001) 1793.
[13] G. Roma, Y. Limoge, L. Martin-Samos, Nucl. Instrum. and Meth. B 250 (2006) 54.